

## Various superstructures formed by tin-vacancy ordering in $\text{K}_8\text{Sn}_{44}\square_2$ and $\text{Rb}_8\text{Sn}_{44}\square_2$ clathrates

Wilder Carrillo-Cabrera, Michael Baitinger, Burcu Uslu and Yuri Grin

Max-Planck-Institut für Chemische Physik fester Stoffe, Dresden, Germany

carrillo@cpfs.mpg.de

Keywords: electron diffraction, vacancy ordering, superstructures, clathrate-I,  $\text{K}_8\text{Sn}_{44}$

The  $\text{K}_8\text{Sn}_{44}\square_2$  and  $\text{Rb}_8\text{Sn}_{44}\square_2$  clathrates are Zintl phases stabilized by creating tin vacancies ( $\square$ ) in the covalent clathrate-I framework [1]. Recently,  $\text{Rb}_8\text{Sn}_{44}\square_2$  [2] and  $\text{Ba}_8\text{Ge}_{43}\square_3$  [3] were reported with partial and full vacancy ordering. Both show the same cubic  $2a_1 \times 2a_1 \times 2a_1$  superstructure (space group  $Ia\bar{3}d$ ), with the vacancies building up a spiral substructure along  $\{100\}$  (similar to that in Fig. 1c).

In contrast to earlier work on  $\text{K}_8\text{Sn}_{44}\square_2$  (Pearson symbol  $cP52$ ,  $a_1 = 12.03 \text{ \AA}$ , space group  $Pm\bar{3}n$ ) [1, 4], in our X-ray powder diffraction (XRPD) patterns splitting of the reflections is observed at high  $2\theta$  values, indicating a non-cubic unit cell. In addition, weak reflections between the main ones revealed the formation of a superstructure. By studying the samples on a Tecnai 10 electron microscope (equipped with CCD camera TemCam-F224HD from TVIPS), selected area electron diffraction SAED patterns show the existence of three different superstructures. The first one is a tetragonal  $2a_1 \times 2a_1 \times 2a_1$  superstructure (SAED patterns in Figs. 1a, 1b) observed in a sample annealed at  $350 \text{ }^\circ\text{C}$  (quenched in water). A suitable crystal structure model ( $a = 24.063(2) \text{ \AA}$ ,  $c = 24.007(2) \text{ \AA}$ ,  $I\bar{4}2d$  space group, Pearson symbol  $tI416$ ) was derived from the structure of  $\text{Ba}_8\text{Ge}_{43}\square_3$ . In this superstructure (see Figs. 1c, 1d), 1.5 of 2 vacancies per formula unit are fully ordered. The pairwise ordering of the majority of the vacancies in the basal plane (Fig. 1d) explains the shortening of the  $c$  axis. The second superstructure has an orthorhombic  $4a_1 \times 2a_1 \times 2a_1$  unit cell ( $oC832$ , SAED patterns in Figs. 2a, 2b) and was found in a furnace cooled sample (after annealing at  $350 \text{ }^\circ\text{C}$ ). The third one is a tetragonal  $4a_1 \times 4a_1 \times 2a_1$  superstructure ( $tI1664$ ; see Figs. 2c, 2d) found in a sample annealed at  $200 \text{ }^\circ\text{C}$  (quenched in water).

TEM study of a  $\text{Rb}_8\text{Sn}_{44}\square_2$  sample annealed at  $400 \text{ }^\circ\text{C}$  (water quenched) revealed a giant orthorhombic  $8a_1 \times 2\sqrt{2}a_1 \times 2\sqrt{2}a_1$  superstructure ( $oC3328$ ; see Fig. 3). Other superstructures related to the  $oC832$  and  $tI1664$  variants in  $\text{K}_8\text{Sn}_{44}\square_2$  were also observed in this  $\text{Rb}_8\text{Sn}_{44}\square_2$  sample. No obvious splitting of the reflections in the high  $2\theta$  region of  $\text{Rb}_8\text{Sn}_{44}\square_2$  XRPD patterns was observed. Thus, it is expected that in the  $\text{Rb}_8\text{Sn}_{44}\square_2$  superstructures the distribution of the tin vacancies is more homogeneous (no vacancy pair structure) than in the  $\text{K}_8\text{Sn}_{44}\square_2$  superstructure variants. Within the same space group, there are at least two different modes for vacancy arrangement.

1. J.T. Zhao, J.D. Corbett, *Inorg. Chem.* 1994, **33**, 5721
2. F. Dubois, T.F. Fässler, *J. Amer. Chem. Soc.* 2005, **127**, 3265.
3. W. Carrillo-Cabrera, S. Budnyk, Yu. Prots, Yu. Grin, *Z. Anorg. Allg. Chem.* 2004, **630**, 2267.
4. J. Gallmeier, H. Schäffer, A. Weiss, *Z. Naturforschung* 1969, **24b**, 665.

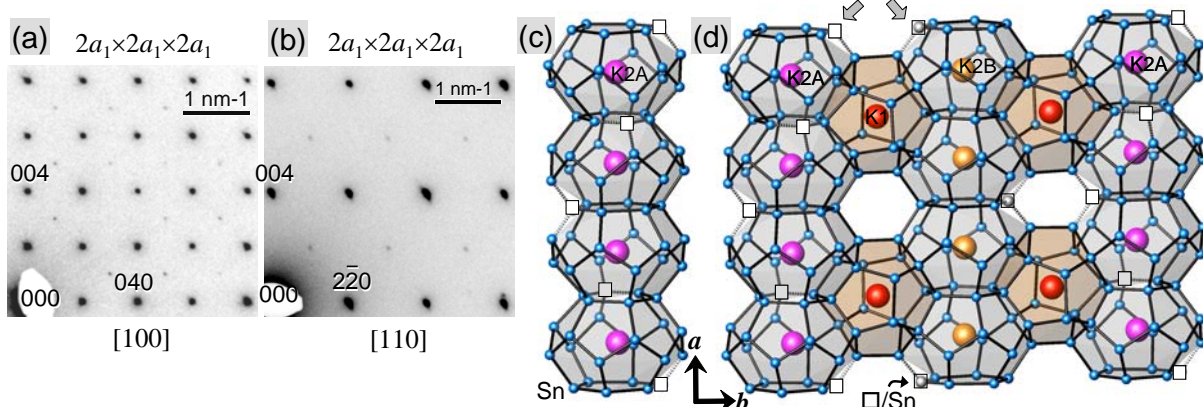


**Figure 1.** (a) [100] and (b) [110] SAED patterns of the *I*-centered tetragonal  $2a_1 \times 2a_1 \times 2a_1$  superstructure (*tI*416) of  $K_8Sn_{44}\square_2$ . (c), (d) Fragments of the  $2a_1 \times 2a_1 \times 2a_1$  structure showing the arrangement of the tin  $\square$  vacancies (spiral substructure along *a* axis in (c)). At short-range level, pairs of vacancies are formed on the basal plane (gray arrows in (d)).

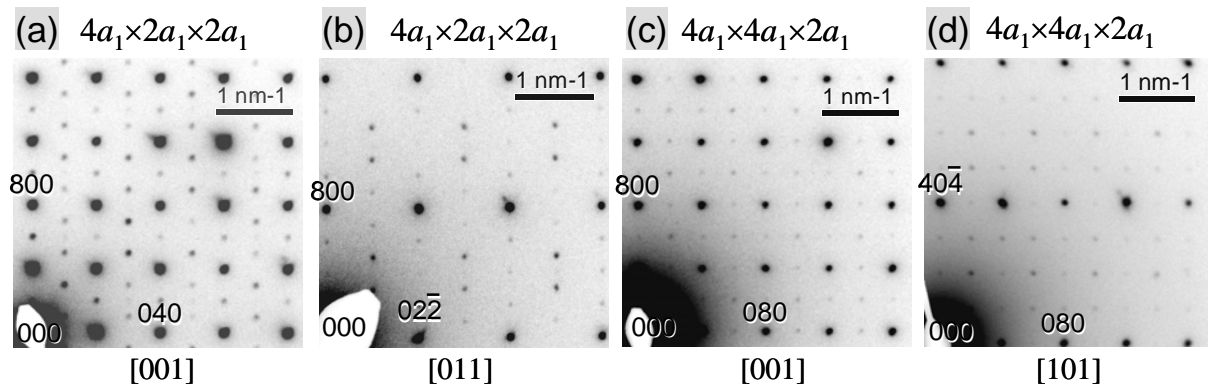


**Figure 2.** (a) [001] and (b) [011] SAED patterns of the orthorhombic  $4a_1 \times 2a_1 \times 2a_1$  superstructure (*oC*832) of  $K_8Sn_{44}\square_2$ . (c) [001] and (d) [101] SAED patterns of the *I*-centered tetragonal  $4a_1 \times 4a_1 \times 2a_1$  superstructure (*tI*1664) of  $K_8Sn_{44}\square_2$ .

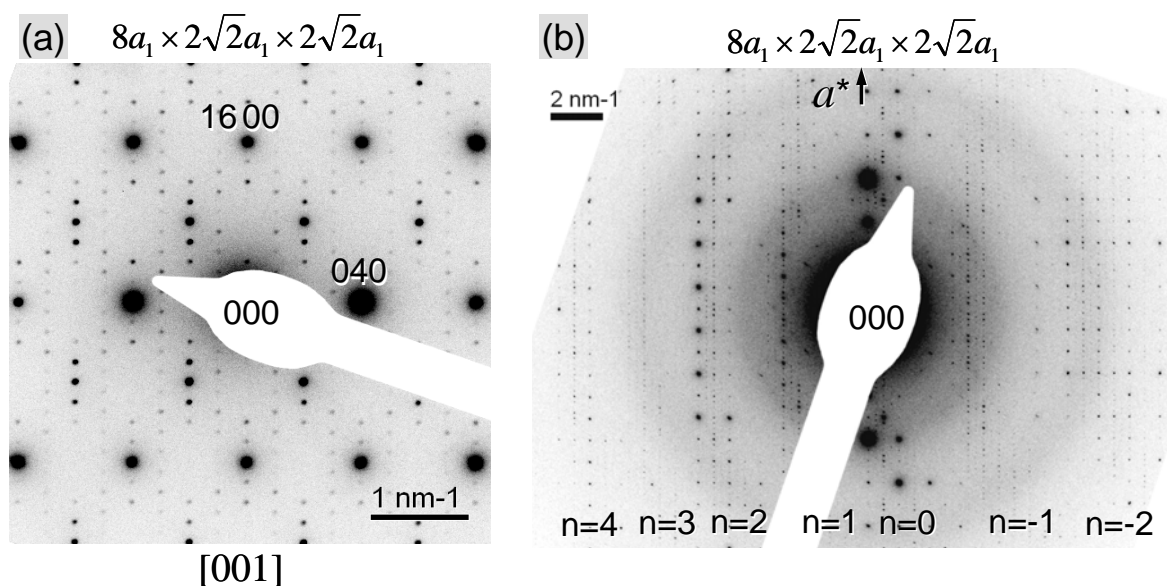


**Figure 3.** (a) [001] SAED pattern of the orthorhombic  $8a_1 \times 2\sqrt{2}a_1 \times 2\sqrt{2}a_1$  superstructure (*oC*3328) of  $Rb_8Sn_{44}\square_2$ . (b) Tilted [001] SAED pattern ( $\sim 6^\circ$  about the  $a^*$  axis), showing the different Laue zones,  $(uvw)_n^*$  layers for  $n = -2, -1, 0, 1, 2, 3, 4$ .